

Dopamine D₁ Receptor Agonist PET Tracer Development: Assessment in Nonhuman Primates

Olivier Barret^{1,2}, Lei Zhang³, David Alagille^{1,4}, Cristian C. Constantinescu¹, Christine Sandiego¹, Caroline Papin¹, Jenna M. Sullivan¹, Thomas Morley¹, Vincent M. Carroll¹, John Seibyl¹, Jianqing Chen⁵, Chewah Lee³, Anabella Villalobos³, David Gray^{3,6}, Timothy J. McCarthy⁵, Gilles Tamagnan^{1,4}

¹Invivo, LLC, New Haven, Connecticut; ²Université Paris-Saclay, CEA, CNRS, MIRCen, Laboratoire des Maladies Neurodégénératives, Fontenay-aux-Roses, France; ³Medicine Design, Medicinal Chemistry, Pfizer Inc., Cambridge, Massachusetts; ⁴Xing Imaging, New Haven, Connecticut; ⁵Digital Medicine and Imaging, Early Clinical Development, Pfizer Inc., Cambridge, Massachusetts; and ⁶Cerevel Therapeutics, Boston, Massachusetts

Non-catechol-based high-affinity selective dopamine D₁ receptor (D1R) agonists were recently described, and candidate PET ligands were selected on the basis of favorable properties. The objective of this study was to characterize in vivo in nonhuman primates 2 novel D1R agonist PET radiotracers, racemic ¹⁸F-MNI-800 and its more active atropisomeric (–)-enantiomer, ¹⁸F-MNI-968. **Methods:** Ten brain PET experiments were conducted with ¹⁸F-MNI-800 on 2 adult rhesus macaques and 2 adult cynomolgus macaques, and 8 brain PET experiments were conducted with ¹⁸F-MNI-968 on 2 adult rhesus macaques and 2 adult cynomolgus macaques. PET data were analyzed with both plasma-input-based methods and reference-region-based methods. Whole-body PET images were acquired with ¹⁸F-MNI-800 from 2 adult rhesus macaques for radiation dosimetry estimates. **Results:** ¹⁸F-MNI-800 and ¹⁸F-MNI-968 exhibited regional uptake consistent with D1R distribution. Specificity and selectivity were demonstrated by dose-dependent blocking with the D₁ antagonist SCH-23390. ¹⁸F-MNI-968 showed a 30% higher specific signal than ¹⁸F-MNI-800, with a nondisplaceable binding potential of approximately 0.3 in the cortex and approximately 1.1 in the striatum. Dosimetry radiation exposure was favorable, with an effective dose of about 0.023 mSv/MBq. **Conclusion:** ¹⁸F-MNI-968 has significant potential as a D1R agonist PET radiotracer, and further characterization in human subjects is warranted.

Key Words: D₁ receptor; agonist; PET imaging; schizophrenia; Parkinson disease;

J Nucl Med 2021; 62:1307–1313
DOI: 10.2967/jnumed.120.256008

Dopamine D₁ receptors (D1Rs) are the most abundant dopamine receptor subtype in the brain and the primary subtype in the prefrontal cortex (1,2) and are exclusively found postsynaptically on dopamine-receptive neurons (medium spiny neurons in the striatum and pyramidal neurons in the prefrontal cortex). Despite its extensive brain distribution, D1R interest has dropped behind other subtypes, especially D₂ receptors, partly because of the lack of

D1R-selective agents that would facilitate a greater understanding of this target.

Dihydropyridine, the first high-affinity catechol-based selective full D1R agonist, demonstrated the therapeutic potential of D1R-selective ligands in schizophrenia (alleviation of cognitive deficit and negative symptoms (3)) and Parkinson disease (antiparkinsonian action in MPTP-treated primate model (4)). The recent introduction of non-catechol-based high-affinity selective D1R agonists has revived interest in this target (5–9).

The development of in vivo imaging techniques has proven extremely valuable to elucidate disease pathology, disease progression, and advancement of target-specific therapies. Several PET radiotracers for D1R have been developed, mainly the antagonists ¹¹C-NNC-112 (10), ¹¹C-SCH-23390 (11), and ¹¹C-A-69024 (12); the partial agonist ¹¹C-N-methyl-NNC 01-0259 (13); and the agonist ¹¹C-SKF 82957 (14). However, ¹¹C-SCH-23390 and ¹¹C-NNC-112 suffer from selectivity against 5-HT_{2a} (15), and ¹¹C-N-methyl-NNC 01-0259 and ¹¹C-SKF 82957 have brain-penetrating radiometabolites (13,14). Moreover, D1Rs exhibit both high- and low-affinity states, with agonists preferentially binding to the high-affinity active state whereas antagonists do not discriminate between the 2 states. Therefore, development of a full D1R agonist PET tracer could provide important in vivo functional information and be a useful imaging tool to assess D1R agonists.

Two novel D1R agonists from a noncatechol chemotype discovered by Pfizer were selected on the basis of favorable properties as potential PET ligands. The objective of this study was to characterize these 2 D1R agonist PET radiotracers, racemic ¹⁸F-MNI-800 and the atropisomeric (–)-enantiomer ¹⁸F-MNI-968, in vivo in nonhuman primates (NHP). We assessed their brain distribution and kinetic profile, the specificity of the signal in preblocking studies with a D1R antagonist and a partial agonist, test–retest variability, and radiation dosimetry estimates of ¹⁸F-MNI-800.

MATERIALS AND METHODS

In Vitro Pharmacology and PET Properties of Novel Noncatechol D1R Agonists

The identification of a suitable PET ligand was guided by a set of PET properties to find a D1R-selective agonist that resides within favorable physicochemical property space defined by the central nervous system PET multiparameter optimization score (>3) (16) and shows potent binding affinity to D1R ($B_{\max}/K_d > 10$), high passive permeability

Received Sep. 28, 2020; revision accepted Dec. 22, 2020.
For correspondence or reprints, contact Olivier Barret (olivier.barret@cea.fr).

Published online February 12, 2021.

COPYRIGHT © 2021 by the Society of Nuclear Medicine and Molecular Imaging.

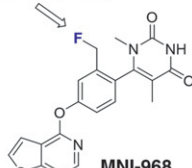
Radiolabeling site	In vitro pharmacology	PET properties
 MNI-968	hD1 K_i = 2 nM	CNS PET MPO = 3.57
	hD1 EC_{50} = 5 nM (96% E_{max})	LogD = 2.2
	rD1 K_i = 8 nM	RRCK P_{app} AB = 21.6×10^{-6} cm/s
	NHP D1 K_i = 2 nM	MDR1 BA/AB = 1.46
	hD2, D3 and D4 binding IC_{50} > 10 μ M	cFu _b = 0.06

FIGURE 1. Profile of D1R agonist PET ligand lead MNI-968. AB = apical to basolateral; BA = basolateral to apical; CNS = central nervous system; cFu_b = fraction unbound in brain; EC_{50} = half-maximal effective concentration; E_{max} = maximal effect; hD1 = human D₁; hD2 = human D₂; IC_{50} = half-maximal inhibitory concentration; K_i = inhibition constant; MDR1 = multi-drug resistance 1; MPO = multiparameter optimization; rD1 = rat D₁; P_{app} = apparent permeability; RRCK = Ralph Russ canine kidney assay.

(RRCK P_{app} AB > 5×10^{-6} cm/s), low p-glycoprotein efflux (Pgp) efflux (MDR1 BA/AB \leq 2.5), and a sufficient fraction unbound in brain (cFu_b > 0.05) for low nonspecific binding.

Initially, racemate MNI-800 (PK-84677) and subsequently its (–)-enantiomer MNI-968 (PF-0110), a noncatechol D1R agonist from a chemotype developed by Pfizer (7), emerged as a promising PET ligand lead with a benzyl fluoride moiety for late-stage 18 F radiolabeling (Fig. 1; Supplemental Scheme 1; supplemental materials are available at <http://jnm.snmjournals.org>).

Indeed, MNI-968 has a potent binding affinity to human D1R (K_i = 2 nM), and minimal species differences in rat (K_i = 8 nM) and NHP (K_i = 2 nM). Given a D1R B_{max} in human and NHP striatum of approximately 52 pmol/g tissue (~52 nM assuming 100 mg of protein/g of tissue) (17), a desired B_{max}/K_d of more than 10 corresponds to a binding affinity of less than 5 nM, indicating that MNI-968 meets this affinity requirement. Moreover, unlike other known D1R antagonist radiotracers (SCH-23390 and NNC-112), MNI-968 is a potent D1R functional agonist with an EC_{50} of 5 nM and 96% E_{max} . Finally, MNI-968 showed selectivity for D1R over other dopamine receptors, with no appreciable binding to human D₂, D₃, and D₄ receptors (IC_{50} > 10 μ M).

In addition to its favorable in vitro pharmacology profile, MNI-968 met all the PET ligand property parameters: high central nervous system PET multiparameter optimization score (3.57), good passive permeability (RRCK P_{app} AB = 21.6×10^{-6} cm/s), low p-glycoprotein efflux (MDR1 BA/AB = 1.46), and a reasonable fraction unbound in brain (cFu_b = 0.06), suggesting a low risk of nonspecific binding.

Details on the synthesis of MNI-968 and MNI-800 are provided in the supplemental materials.

Radiochemistry of 18 F-MNI-800 and 18 F-MNI-968

All 18 F-MNI-800 and 18 F-MNI-968 radiolabeling reactions were performed in a GE Healthcare TRACERlab FX-FN automated synthesis module using the Boc-protected benzyl chloride precursor (Fig. 2, MNI-799 or MNI-969).

For 18 F-MNI-800, the 2-step, 1-pot production with the racemic precursor MNI-799 afforded sufficiently high yields (15%–35%) with high radiochemical purity (>95%), chemical purity (<0.20 μ g/mL), and specific activity (>220 GBq/ μ mol).

For 18 F-MNI-968, it proved too difficult to confidently control the undesired racemization of the enantiopure precursor MNI-969, and the procedure was modified. First, an in-process chiral high-performance liquid chromatography separation step with inclusion of a chiral column before the C18 reverse-phase column provided sequential separation of the desired atropisomer followed by mass purification. Second, the radiolabeling solvent was changed to acetonitrile because dimethyl sulfide was not compatible with the chiral stationary phase. Beyond these 2 changes, the 18 F-MNI-968 process was similar to the process for 18 F-MNI-800 and provided the desired product in expected lower yields (5%–15%) and an acceptable chemical profile (radiochemical purity

> 95%, chemical purity < 0.10 μ g/mL, and specific activity > 75 GBq/ μ mol). Atropisomeric purity was assessed to confirm enantiopurities of more than 99% at the end of synthesis, throughout storage in solution, and before injection.

Details on the radiosynthesis of 18 F-MNI-800 and 18 F-MNI-968 are provided in the supplemental materials.

Animals

All experiments were conducted in accordance with the U.S. Public Health Service's Policy on Humane Care and Use of Laboratory Animals and with institutional approval (Yale PET Center and Charles River Laboratories). Adult rhesus macaques (*Macaca mulatta*, 2 females [7.6 \pm 1.4 kg, NHPs A and B] and 1 male [19.6 \pm 3.0 kg, NHP C]) and cynomolgus macaques (*Macaca fascicularis*, 3 males, 5.0 \pm 0.4 kg, NHPs D–F) were studied. The animals were anesthetized with intramuscular ketamine and given glycopyrrolate to reduce secretions, transferred to the camera, and intubated for continuous anesthesia with approximately 2.5% isoflurane. Radiotracer was injected 2 h after administration of anesthetics to allow for stabilization of the animals' physiology. Body temperature was maintained by a heated water blanket and monitored with a rectal thermometer.

Blocking Agent Preparation and Administration

SCH-23390 (R(+)-SCH-23390 hydrochloride; Sigma-Aldrich) and PF-2562 (8,9) are a potent, selective D1R antagonist and a partial agonist, respectively. SCH-23390 was dissolved in normal saline. PF-2562 was dissolved in 5% ethanol, 5% Cremophor (BASF Corp.), and 18.5% sulfolbutylether- β -cyclodextrin in sterile water.

Receptor occupancy experiments were performed with 18 F-MNI-800 and 4 doses of SCH-23390 (0.03, 0.1, 0.2, and 0.5 mg/kg) administered intravenously over a 20-min period beginning 25 min before the radiotracer injection, and with 18 F-MNI-968 and 1 dose of PF-2562 in duplicate (1.2 mg/kg total dose) administered intravenously over a 120-min period beginning 30 min before tracer injection (bolus of 0.121 mg/kg/min for 3 min followed by infusion of 0.007 mg/kg/min for 117 min). Plasma samples were taken at several time points during each PET scan.

Brain PET Studies

PET scans were performed on a Focus 220 microPET camera (Siemens Healthcare Molecular Imaging) after intravenous bolus administration of 18 F-MNI-800 (170.5 \pm 16.5 MBq, 0.28 \pm 0.22 μ g) or 18 F-MNI-968 (158.0 \pm 29.1 MBq, 0.47 \pm 0.22 μ g). Ten scans were done with 18 F-MNI-800, and 8 scans were done with 18 F-MNI-968 (Table 1). Test and retest scans were separated by 2 wk for 18 F-MNI-800 and 4 mo for 18 F-MNI-968. The dynamic series were reconstructed using filtered backprojection with corrections for random, scatter, and attenuation.

Arterial Input Function. After tracer administration, radial artery blood samples were collected over 2 h. Radioactivity in whole blood and plasma was measured in all samples. Radiometabolites were

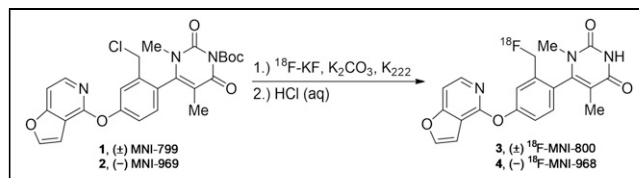


FIGURE 2. Radiosynthesis of 18 F-MNI-800 and 18 F-MNI-968.

TABLE 1
Summary of Scans with ^{18}F -MNI-800 or ^{18}F -MNI-968

Species	NHP no.	^{18}F -MNI-800	^{18}F -MNI-968
Rhesus	A	Test, retest, SCH23390 (0.5 and 0.1 mg/kg)	Test, retest,* PF-2562 (1.2 mg/kg)*
	B	Test, retest, SCH23390 (0.2 and 0.03 mg/kg), dosimetry	Baseline
	C	Dosimetry	Baseline,* PF-2562 (1.2 mg/kg)*
Cynomolgus	D	Baseline	Baseline
	E	Baseline	
	F		Baseline

*90-min scan.
Scans are 120 min unless otherwise indicated.

measured in a subset of samples by reverse-phase high-performance liquid chromatography performed on a Phenomenex Luna C18(2) (10×250 mm, $10 \mu\text{m}$) at a flow rate of 4 mL/min. The mobile phase consisted of a mixture of methanol/water with 0.2% triethylamine in a 65/35 ratio. Plasma samples were processed by acetonitrile denaturation, and the plasma protein binding free fraction (f_p) was measured by ultrafiltration (Centrifree; Millipore).

Image Processing. PET images were analyzed in PMOD, version 3.609 (PMOD Technologies), and were motion-corrected frame by frame when necessary. The initial PET images (15 min) were averaged and aligned onto a rhesus or cynomolgus structural T1-weighted MRI template, and the transformation matrix was applied to the whole PET series. A volume-of-interest atlas (including the caudate, putamen, globus pallidus, nucleus accumbens, thalamus, cortical regions, and cerebellum) was applied to the PET series in MRI rhesus or cynomolgus template space to extract the regional time-activity curves. Curves were expressed in SUV by normalizing the activity concentration by the injected dose and animal body weight.

Kinetic Modeling and Analysis. Time-activity curves were analyzed with 1- and 2-tissue-compartment (2T) models (18) and Logan graphical analysis (LGA) (19) using the arterial plasma input function corrected for radiometabolites to derive the volume of distribution (V_T) and the influx rate constant K_1 in each region. The nondisplaceable binding potential (BP_{ND}) was estimated using the cerebellum as a reference region: $\text{BP}_{\text{ND}} = V_T/V_{\text{ND}} - 1$, V_T and V_{ND} being the distribution volumes in the target region (specific and nondisplaceable binding) and reference region (nondisplaceable binding), respectively (20). In addition, BP_{ND} was directly derived from the simplified reference tissue model (SRTM) (21) and noninvasive LGA (NI-LGA) (19) with the cerebellum as a reference region. All kinetic analyses were performed using PMOD. Test-retest variability for V_T and BP_{ND} was estimated as absolute (test - retest)/average (test + retest).

The D1R occupancy (Occ) produced by SCH-23390 or PF-2562 was determined as the percentage change in BP_{ND} : $\text{Occ} = (\text{BP}_{\text{ND}}^{\text{baseline}} - \text{BP}_{\text{ND}}^{\text{drug}}) / \text{BP}_{\text{ND}}^{\text{baseline}}$. The SCH-23390 plasma-occupancy curves for the striatum (putamen and caudate) were fitted in Prism (version 6.01; GraphPad Software) with a single specific binding site model: $\text{Occ} = \text{Occ}_{\text{max}} \times C / (C + \text{EC}_{50})$, where Occ_{max} is the maximum occupancy; EC_{50} is the half-maximal effective concentration, which represents the SCH-23390 plasma level for 50% occupancy; and C represents the SCH-23390 average plasma level during the scan.

^{18}F -MNI-800 Whole-Body PET Studies

Two adult rhesus monkeys (*Macaca mulatta*), 1 male and 1 female, were used for whole-body PET imaging from head to mid thigh over 4 h on a Biograph mCT PET/CT camera (Siemens Healthcare Molecular

Imaging) after intravenous bolus injection of ^{18}F -MNI-800 to determine the biodistribution and estimate absorbed radiation doses.

PET images were imported into PMOD, and volumes of interest were drawn on source organs. Absorbed radiation dose and effective dose (International Commission on Radiological Protection publication 60) were estimated with OLINDA/EXM software, version 1.0 (22), according to the male or female model. The gastrointestinal model of International Commission on Radiological Protection publication 30 was used with the assumption that activity entered the gastrointestinal tract through the small intestine (fraction of activity entering the intestine was estimated as the highest fraction encountered in the intestinal area).

RESULTS

Plasma Analysis

High-performance liquid chromatography analysis of ^{18}F -MNI-800 and ^{18}F -MNI-968 arterial plasma revealed 1 major radiometabolite and 1 minor metabolite eluting just after the first one (whose contribution remained small throughout the study), with both metabolites more polar than the parent compound. No difference was observed between rhesus and cynomolgus macaques, and the results were pooled across the 2 species. ^{18}F -MNI-800 and ^{18}F -MNI-968 showed similar moderate metabolic profiles, with about 60%–70% and 40%–50% of intact parent remaining at 30 and 120 min after

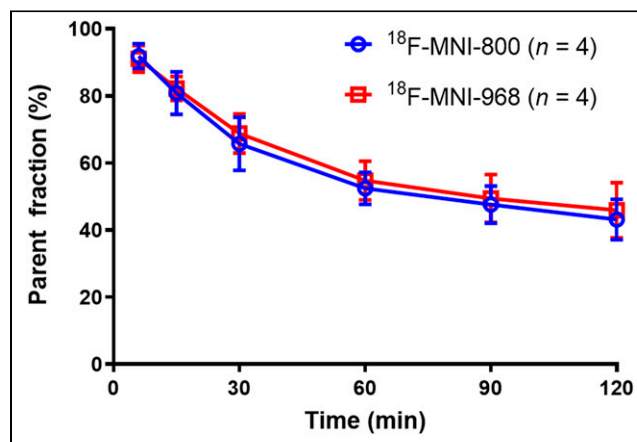


FIGURE 3. Parent fraction profile in arterial plasma after intravenous administration of ^{18}F -MNI-800 (mean \pm SD, $n = 4$) or ^{18}F -MNI-968 (mean \pm SD, $n = 4$).

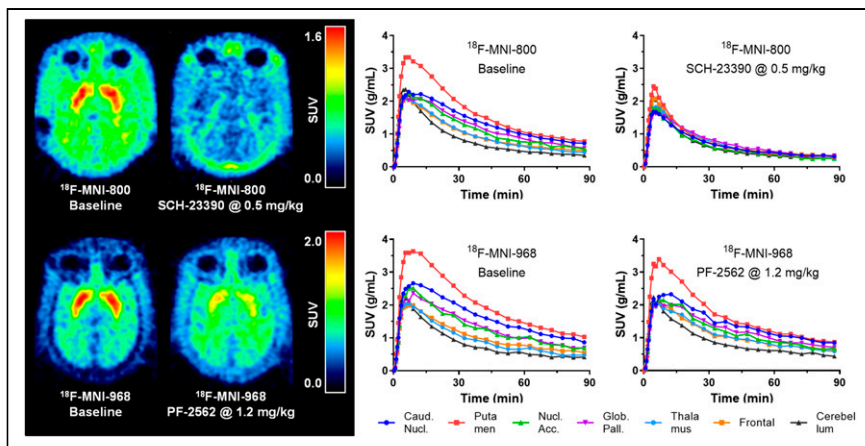


FIGURE 4. (Left) Average PET images from 30 to 90 min after injection for rhesus macaque (NHP A) in transverse plane of ^{18}F -MNI-800 at baseline and after dosing with SCH-23390 at 0.5 mg/kg (occupancy of $\sim 85\%$) and of ^{18}F -MNI-968 at baseline and after dosing with PF-2562 at 1.2 mg/kg (occupancy of $\sim 40\%$). (Right) Time-activity curves in some brain regions for same rhesus macaque for studies with ^{18}F -MNI-800 and ^{18}F -MNI-968. Caud. Nucl. = caudate nucleus; Glob. Pall. = globus pallidus; Nucl. Acc. = nucleus accumbens.

injection, respectively (Fig. 3). Plasma parent f_p measured by ultrafiltration was $13.4\% \pm 1.3\%$ ($n = 4$) for ^{18}F -MNI-800 and $13.5\% \pm 1.5\%$ ($n = 4$) for ^{18}F -MNI-968.

Brain Uptake Distribution and Time-Activity Curves

Representative average ^{18}F -MNI-968 and ^{18}F -MNI-800 PET images in a rhesus macaque at baseline showed the highest uptake in the striatum, consistent with known D1R distribution (Fig. 4, left). The ^{18}F -MNI-800 PET image after a SCH-23390 preblock (0.5 mg/kg) demonstrated almost complete saturation. ^{18}F -MNI-968 and ^{18}F -MNI-800 time-activity curves at baseline and after a SCH-23390 (0.5 mg/kg) or PF-2562 (1.2 mg/kg) preblock are presented in Figure 4 (right) in the same rhesus macaque. Both ^{18}F -MNI-968 and ^{18}F -MNI-800 readily entered the brain, with SUV_{peak} at 5–10 min after injection. The signal was highest in the putamen and caudate nucleus, followed by the globus pallidus and nucleus accumbens, with the lowest uptake consistently found in the cerebellum. Clear blocking of ^{18}F -MNI-800 or ^{18}F -MNI-968 uptake was seen after preblocking with SCH-23390 (0.5 mg/kg, occupancy of $\sim 85\%$) or PF-2562 (1.2 mg/kg, occupancy of $\sim 40\%$), respectively. Higher uptake was also observed for ^{18}F -MNI-968 than for ^{18}F -MNI-800, particularly in the putamen and caudate nucleus, whereas a similar profile was maintained in the cerebellum.

Kinetic Analysis

2T was favored for both ^{18}F -MNI-800 and ^{18}F -MNI-968 data over 1 tissue compartment based on the Akaike information criterion. Typical 2T and SRTM fits and Logan plots (LGA with $t^* = 15$ min, and NI-LGA with $t^* = 10$ min) are provided in Figure 5 for a baseline study in a rhesus macaque with ^{18}F -MNI-968. SRTM determined k'_2 to be $0.17 \pm 0.04 \text{ min}^{-1}$ ($n = 4$) for ^{18}F -MNI-800 and $0.16 \pm 0.02 \text{ min}^{-1}$ ($n = 5$) for ^{18}F -MNI-968, and these SRTM estimates of k'_2 were used for the NI-LGA fit.

A within-animal comparison ($n = 2$) between ^{18}F -MNI-800 and ^{18}F -MNI-968 V_T estimates (2T model) is shown in Figure 6A and indicates a higher specific signal for ^{18}F -MNI-968 (negative y-intercept) and the same target/ B_{max} for both tracers (linearity of the relationship) (23). Since the f_p was similar for ^{18}F -MNI-800 and ^{18}F -MNI-968, the slope corresponds to the in vivo affinities ratio

and predicts a K_d about 1.3 times higher for ^{18}F -MNI-800 (23). Furthermore, V_T in the cerebellum was $1.83 \pm 0.06 \text{ mL/cm}^3$ for ^{18}F -MNI-800, compared with $1.87 \pm 0.01 \text{ mL/cm}^3$ for ^{18}F -MNI-968, demonstrating a similar nondisplaceable signal for both tracers, with a relationship with BP_{ND} (2T model) for the within-animal studies: $\text{BP}_{\text{ND}}(\text{MNI-968}) = 1.29 \times \text{BP}_{\text{ND}}(\text{MNI-800}) + 0.006$.

Figures 6B and 6C compare V_T and BP_{ND} across methods for ^{18}F -MNI-968, demonstrating very good agreement between the different estimates ($R^2 = 0.99$), in particular for BP_{ND} between plasma-based and reference region-based methods, with points aligning almost on the identity line. Similar results were obtained for ^{18}F -MNI-800 (data not shown). A summary of V_T and BP_{ND} for the different methods is provided for a subset of regions in Table 2 for ^{18}F -MNI-800

($n = 4$) and in Table 3 for ^{18}F -MNI-968 ($n = 3$ for 2T and LGA, and $n = 5$ for SRTM and NI-LGA). Additional kinetic parameters for 2T are provided in Supplemental Tables 1 and 2. V_T ranged from approximately $1.9 \pm 0.1 \text{ mL/cm}^3$ in the cerebellum (similar estimates for both tracers) to approximately $3.7 \pm 0.3 \text{ mL/cm}^3$ and $4.3 \pm 0.2 \text{ mL/cm}^3$ in the putamen for ^{18}F -MNI-800 and ^{18}F -MNI-968, respectively. BP_{ND} ranged from approximately 0.2 in the cortex to 0.9 in the putamen for ^{18}F -MNI-800, and from approximately 0.3 in the cortex to 1.1–1.2 in the putamen for ^{18}F -MNI-968, confirming an average specific signal higher by approximately 30%. K_1 (2T model) was similar across regions, animals, and tracers, with $K_1 = 0.23 \pm 0.03 \text{ mL}\cdot\text{cm}^{-3}\cdot\text{min}^{-1}$ for ^{18}F -MNI-800 and $K_1 = 0.27 \pm 0.06 \text{ mL}\cdot\text{cm}^{-3}\cdot\text{min}^{-1}$ for ^{18}F -MNI-968 (Supplemental Tables 1 and 2).

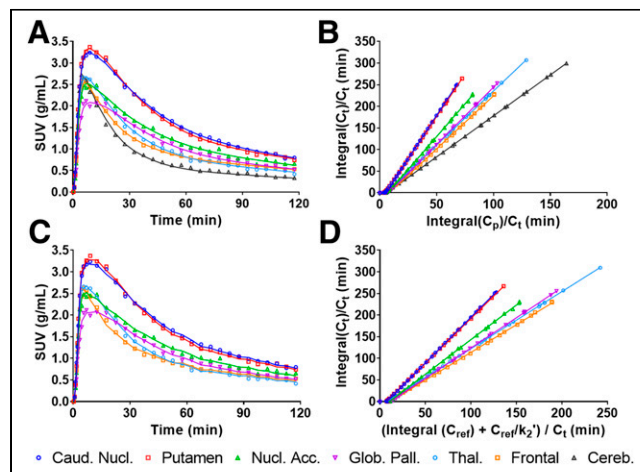


FIGURE 5. (A and C) Representative time-activity curves at baseline for rhesus macaque (NHP B) in some brain regions after bolus injection of ^{18}F -MNI-968, showing 2T compartment model fits (A) and SRTM fits (C). (B and D) Graphical analysis with LGA with plasma input function ($t^* = 15$ min) (B) and NI-LGA with reference region input function ($t^* = 10$ min) (D). Caud. Nucl. = caudate nucleus; C_p = activity concentration in plasma; C_{ref} = activity concentration in reference region; C_i = activity concentration in region of interest; Glob. Pall. = globus pallidus; Nucl. Acc. = nucleus accumbens; Thal. = thalamus.

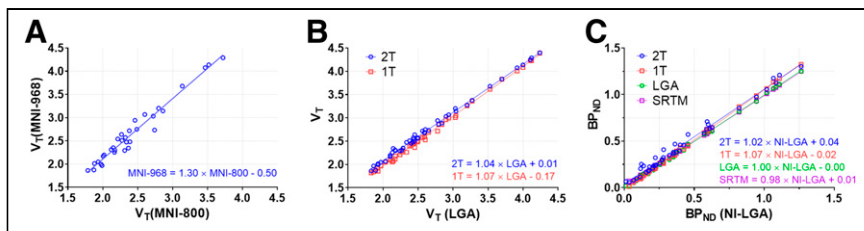


FIGURE 6. (A) Within-animal comparison ($n = 2$) of ^{18}F -MNI-800 and ^{18}F -MNI-968 2T V_T estimates. (B) Comparison of ^{18}F -MNI-968 V_T estimates across models ($n = 3$). (C) Comparison of ^{18}F -MNI-968 BP_{ND} estimates across models ($n = 3$). 1T = 1 tissue compartment.

Test–retest variability was assessed in a limited number of repeat studies for ^{18}F -MNI-800 ($n = 2$) and ^{18}F -MNI-968 ($n = 1$). The results are summarized in Supplemental Tables 3 and 4 for the different methods. Variability in V_T estimates was low in all regions and both tracers ($<10\%$), whereas that of BP_{ND} in the striatum remained low for ^{18}F -MNI-800 ($<5\%$) and somewhat higher for ^{18}F -MNI-968 ($\sim 15\%$), for which, however, test and retest scans were separated by 4 mo.

SCH-23390 Occupancy Studies

Preblocking with SCH-23390 increased the measured occupancies in a dose-dependent fashion and reduced the ^{18}F -MNI-800 uptake to levels close to those in the cerebellum at the highest dose tested (Fig. 4), supporting the specificity and selectivity of ^{18}F -MNI-800 for D1R, with measured occupancies of approximately 85% and 60% at the 2 highest SCH-23390 doses of 0.5 and 0.2 mg/kg, respectively.

SCH-23390 plasma levels during the preblocking studies are shown in Figure 7A, and the relationship between the measured D1R occupancy and the average plasma levels during the PET imaging (25–145 min after administration of SCH-23390) is shown in Figure 7B for the various analysis methods used, for which the maximum occupancy was constrained to 100%. All methods produced similar occupancy measurements, with slightly lower estimates for 2T at the 2 lowest SCH-23390 doses, with a consistent estimated EC_{50} ranging from 6.0 ± 1.0 ng/mL for NI-LGA to 8.5 ± 1.0 ng/mL for 2T (average, ~ 7 ng/mL).

^{18}F -MNI-800 Dosimetry

Whole-body studies showed that ^{18}F -MNI-800 is eliminated mainly via the hepatobiliary route. The urinary bladder, gallbladder, and liver were determined to be the critical organs with the highest absorbed dose (Supplemental Table 5). The whole-body effective dose (ED) was estimated to be 0.025 mSv/MBq for the female rhesus and 0.021 mSv/MBq for the male rhesus, in line with other ^{18}F -labeled tracers (e.g., 0.019 mSv/MBq for ^{18}F -FDG (24)).

DISCUSSION

Both ^{18}F -MNI-800 and its active atropisomeric (–)-enantiomer ^{18}F -MNI-968 demonstrated high penetration in monkey brain, with uptake distribution in agreement with the known D1R distribution. Blood profiles were highly similar, with an almost identical metabolism rate and f_p ($\sim 13\%$).

SCH-23390 has a 5-HT_{2a} component (15); however, the density of 5-HT_{2a} receptors in the striatum is negligible compared with D1R. Therefore, SCH-23390 preblocking studies confirmed the specificity and selectivity of ^{18}F -MNI-800 for D1R over other targets in

the striatum, as is expected to hold true for ^{18}F -MNI-968 because it is one enantiomer. Absolute selectivity against 5-HT_{2a} receptors could be tested further by a challenge with the selective 5-HT_{2a} antagonist MDL 100907. These studies also confirmed the choice of the cerebellum as a reference region for non-invasive methods, BP_{ND} calculations, and occupancy measurements since the signal in this region was not blocked. This choice is also supported by a V_{ND} estimate from occupancy plots of 2.0 ± 0.1 (25), in very good

agreement with a V_T of 1.9 ± 0.1 in the cerebellum (Table 2). Assuming passive diffusion through the blood–brain barrier, the tissue non-displaceable free fraction (f_{ND}) can be calculated from the measured f_p and V_{ND} above (20), giving an f_{ND} of approximately 7%, in close agreement with the unbound fraction of 6% in brain. Finally, the agreement in occupancy estimates between the plasma-based and reference-region-based methods suggests that D1R occupancy can be quantitatively assessed in monkeys using SRTM or NI-LGA, without the need for arterial sampling.

BP_{ND} in humans and NHPs was reported to be approximately 0.4–0.6 in the cortex and 2.0–3.0 in the striatum for ^{11}C -SCH-23390 and approximately 0.6–0.8 in the cortex and 3.0–4.0 in the striatum for ^{11}C -NNC-112 (15,26–28), which are higher than the values reported here for ^{18}F -MNI-968 (~ 0.3 in the cortex and ~ 1.1 in the striatum, Table 3). Also, BP_{ND} variability in humans was reported as approximately 10%–15% in the cortex and 5.0%–10% in the striatum for both ^{11}C -SCH-23390 and ^{11}C -NNC-112 (27,29), marginally better than that reported here (Supplemental Table 3), although we assessed the variability in a limited number of animals. However, both ^{11}C -SCH-23390 and ^{11}C -NNC-112 are antagonist radioligands and therefore cannot provide information on the high- or low-affinity state of D1R, and both suffer from a cortical 5-HT_{2a} signal that represents about 20%–30% of the total signal (15,26). Therefore, further evaluation and characterization of ^{18}F -MNI-968 in human subjects is warranted because the tracer could prove to be a valuable tool in Parkinson disease (9) and in psychiatric disorders such as schizophrenia (8).

CONCLUSION

We report here the evaluation of racemate ^{18}F -MNI-800 and its (–)-enantiomer ^{18}F -MNI-968 in NHPs. Both tracers had regional uptake consistent with D1R distribution. The selectivity and

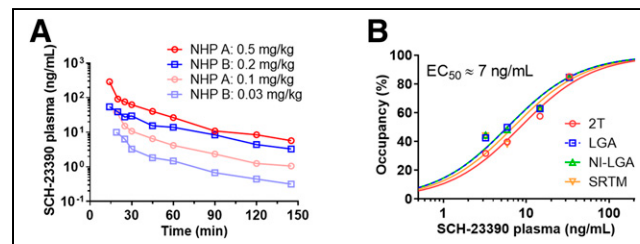


FIGURE 7. (A) SCH-23390 plasma levels for 4 doses, with ^{18}F -MNI-800 injection at 25 min after drug administration. (B) Striatal D1R occupancy against average plasma levels between 25 and 145 min after administration of SCH-23390. EC_{50} = half-maximal effective concentration.

TABLE 2
¹⁸F-MNI-800 V_T and BP_{ND} in Pooled Rhesus and Cynomolgus Macaques

Region	V _T		BP _{ND}			
	2T	LGA	2T	LGA	SRTM	NI-LGA
Striatum	3.6 ± 0.3 (8%)	3.5 ± 0.3 (8%)	0.86 ± 0.10 (11%)	0.83 ± 0.08 (9%)	0.83 ± 0.07 (8%)	0.83 ± 0.07 (8%)
Caudate	3.5 ± 0.4 (11%)	3.4 ± 0.4 (11%)	0.81 ± 0.11 (14%)	0.78 ± 0.10 (12%)	0.78 ± 0.09 (11%)	0.78 ± 0.09 (12%)
Putamen	3.7 ± 0.3 (7%)	3.6 ± 0.3 (7%)	0.91 ± 0.14 (15%)	0.88 ± 0.12 (13%)	0.89 ± 0.11 (12%)	0.89 ± 0.11 (13%)
Nucleus accumbens	2.9 ± 0.2 (7%)	2.8 ± 0.2 (7%)	0.48 ± 0.03 (6%)	0.46 ± 0.02 (5%)	0.45 ± 0.02 (5%)	0.46 ± 0.02 (5%)
Globus pallidus	2.9 ± 0.3 (9%)	2.8 ± 0.3 (9%)	0.50 ± 0.06 (13%)	0.48 ± 0.06 (12%)	0.48 ± 0.06 (12%)	0.48 ± 0.05 (11%)
Thalamus	2.4 ± 0.2 (9%)	2.4 ± 0.2 (8%)	0.25 ± 0.06 (22%)	0.25 ± 0.04 (17%)	0.26 ± 0.04 (16%)	0.26 ± 0.04 (16%)
Frontal cortex	2.3 ± 0.0 (0%)	2.2 ± 0.0 (1%)	0.24 ± 0.04 (18%)	0.20 ± 0.05 (24%)	0.20 ± 0.05 (23%)	0.20 ± 0.05 (25%)
Cerebellum	1.9 ± 0.1 (7%)	1.9 ± 0.1 (6%)				

Data are mean ± SD, followed by coefficient of variation in parentheses (*n* = 4).

specificity of ¹⁸F-MNI-800 and ¹⁸F-MNI-968 for D1R were demonstrated against SCH-23390 or PF-2562, a selective D1R antagonist and a partial agonist, respectively. Noninvasive quantification of ¹⁸F-MNI-800 and ¹⁸F-MNI-968 with SRTM or LGA using the cerebellum as a reference is possible, particularly for occupancy studies. ¹⁸F-MNI-800 dosimetry, and putatively dosimetry of ¹⁸F-MNI-968, are favorable, with an effective dose consistent with values reported for other PET radiotracers. Therefore, ¹⁸F-MNI-968 has great potential as a D1R agonist PET radiotracer and warrants further characterization in human subjects.

DISCLOSURE

The research reported in this publication was supported by the National Institute of Mental Health of the National Institutes of Health under award U01MH107803. No other potential conflict of interest relevant to this article was reported.

ACKNOWLEDGMENTS

We thank Dr. Richard Carson and the staff at the Yale PET Center for conducting the rhesus monkey experiments.

KEY POINTS

QUESTION: Does the agonist PET tracer ¹⁸F-MNI-968 show suitable properties and specific binding to quantify D₁ dopamine receptor?

PERTINENT FINDINGS: ¹⁸F-MNI-968, the atropisomeric (–)-enantiomer, showed a suitable in vitro pharmacology profile, high brain uptake, favorable kinetics, and specific binding that was blocked by a selective D1R antagonist and a partial agonist.

IMPLICATIONS FOR PATIENT CARE: ¹⁸F-MNI-968 has potential as an agonist PET radioligand to quantify D1Rs in the high-affinity state in human brains, particularly in neurologic and psychiatric disorders.

TABLE 3
¹⁸F-MNI-968 V_T and BP_{ND} in Pooled Rhesus and Cynomolgus Macaques

Region	V _T		BP _{ND}			
	2T	LGA	2T	LGA	SRTM	NI-LGA
Striatum	4.1 ± 0.2 (4%)	4.0 ± 0.2 (4%)	1.14 ± 0.05 (5%)	1.07 ± 0.02 (2%)	1.07 ± 0.03 (2%)	1.08 ± 0.03 (3%)
Caudate	4.0 ± 0.3 (8%)	3.9 ± 0.3 (8%)	1.08 ± 0.12 (11%)	1.02 ± 0.09 (9%)	1.06 ± 0.09 (8%)	1.06 ± 0.08 (8%)
Putamen	4.3 ± 0.2 (4%)	4.1 ± 0.2 (4%)	1.20 ± 0.09 (8%)	1.13 ± 0.10 (9%)	1.11 ± 0.08 (7%)	1.12 ± 0.08 (8%)
Nucleus accumbens	3.2 ± 0.2 (5%)	3.1 ± 0.2 (6%)	0.65 ± 0.02 (4%)	0.61 ± 0.00 (0%)	0.59 ± 0.07 (12%)	0.60 ± 0.07 (12%)
Globus pallidus	3.2 ± 0.6 (18%)	3.1 ± 0.5 (18%)	0.65 ± 0.20 (31%)	0.60 ± 0.21 (35%)	0.58 ± 0.18 (31%)	0.58 ± 0.18 (31%)
Thalamus	2.6 ± 0.2 (9%)	2.6 ± 0.2 (9%)	0.35 ± 0.04 (13%)	0.33 ± 0.04 (13%)	0.29 ± 0.05 (19%)	0.29 ± 0.06 (20%)
Frontal cortex	2.6 ± 0.1 (2%)	2.4 ± 0.1 (2%)	0.33 ± 0.08 (25%)	0.27 ± 0.04 (15%)	0.28 ± 0.05 (17%)	0.28 ± 0.05 (18%)
Cerebellum	1.9 ± 0.1 (6%)	1.9 ± 0.1 (5%)				

Data are mean ± SD, followed by coefficient of variation in parentheses (*n* = 3 for 2T and LGA, and *n* = 5 for SRTM and NI-LGA).

REFERENCES

- Hall H, Sedvall G, Magnusson O, Kopp J, Halldin C, Farde L. Distribution of D1- and D2-dopamine receptors, and dopamine and its metabolites in the human brain. *Neuropsychopharmacology*. 1994;11:245–256.
- Meador-Woodruff JH, Damask SP, Wang J, Haroutunian V, Davis KL, Watson SJ. Dopamine receptor mRNA expression in human striatum and neocortex. *Neuropsychopharmacology*. 1996;15:17–29.
- Rosell DR, Zaluda LC, McClure MM, et al. Effects of the D1 dopamine receptor agonist dihydrexidine (DAR-0100A) on working memory in schizotypal personality disorder. *Neuropsychopharmacology*. 2015;40:446–453.
- Schneider JS, Sun ZQ, Roeltgen DP. Effects of dihydrexidine, a full dopamine D-1 receptor agonist, on delayed response performance in chronic low dose MPTP-treated monkeys. *Brain Res*. 1994;663:140–144.
- Kozak R, Kiss T, Dlugolenski K, et al. Characterization of PF-6142, a novel, non-catecholamine dopamine receptor D1 agonist, in murine and nonhuman primate models of dopaminergic activation. *Front Pharmacol*. 2020;11:1005.
- Hall A, Provins L, Valade A. Novel strategies to activate the dopamine D1 receptor: recent advances in orthosteric agonism and positive allosteric modulation. *J Med Chem*. 2019;62:128–140.
- Coe JW, Allen JA, Davoren JE, et al., inventors; Pfizer Inc., assignee. Heteroaromatic compounds and their use as dopamine D1 ligands. International patent WO2014072881 A1. 2014.
- Arce E, Balice-Gordon R, Duvvuri S, et al. A novel approach to evaluate the pharmacodynamics of a selective dopamine D1/D5 receptor partial agonist (PF-06412562) in patients with stable schizophrenia. *J Psychopharmacol*. 2019;33:1237–1247.
- Papapetropoulos S, Liu W, Duvvuri S, Thayer K, Gray DL. Evaluation of D1/D5 partial agonist PF-06412562 in Parkinson's disease following oral administration. *Neurodegener Dis*. 2018;18:262–269.
- Halldin C, Foged C, Chou YH, et al. Carbon-11-NNC 112: a radioligand for PET examination of striatal and neocortical D1-dopamine receptors. *J Nucl Med*. 1998;39:2061–2068.
- Halldin C, Stone-Elander S, Farde L, et al. Preparation of ¹¹C-labelled SCH 23390 for the in vivo study of dopamine D-1 receptors using positron emission tomography. *Int J Rad Appl Instrum [A]*. 1986;37:1039–1043.
- Kassiou M, Scheffel U, Ravert HT, et al. [¹¹C]A-69024: a potent and selective non-benzazepine radiotracer for in vivo studies of dopamine D1 receptors. *Nucl Med Biol*. 1995;22:221–226.
- Finnema SJ, Bang-Andersen B, Jorgensen M, et al. The dopamine D₁ receptor agonist (S)-[¹¹C]N-methyl-NNC 01-0259 is not sensitive to changes in dopamine concentration: a positron emission tomography examination in the monkey brain. *Synapse*. 2013;67:586–595.
- Palmer M, McCormick P, Parkes J, Knudsen GM, Wilson AA. Systemic catechol-O-methyl transferase inhibition enables the D1 agonist radiotracer R-[¹¹C]SKF 82957. *Nucl Med Biol*. 2010;37:837–843.
- Ekelund J, Slifstein M, Narendran R, et al. In vivo DA D₁ receptor selectivity of NNC 112 and SCH 23390. *Mol Imaging Biol*. 2007;9:117–125.
- Zhang L, Villalobos A, Beck EM, et al. Design and selection parameters to accelerate the discovery of novel central nervous system positron emission tomography (PET) ligands and their application in the development of a novel phosphodiesterase 2A PET ligand. *J Med Chem*. 2013;56:4568–4579.
- Cumming P. Absolute abundances and affinity states of dopamine receptors in mammalian brain: a review. *Synapse*. 2011;65:892–909.
- Slifstein M, Laruelle M. Models and methods for derivation of in vivo neuroreceptor parameters with PET and SPECT reversible radiotracers. *Nucl Med Biol*. 2001;28:595–608.
- Logan J. A review of graphical methods for tracer studies and strategies to reduce bias. *Nucl Med Biol*. 2003;30:833–844.
- Innis RB, Cunningham VJ, Delforge J, et al. Consensus nomenclature for in vivo imaging of reversibly binding radioligands. *J Cereb Blood Flow Metab*. 2007;27:1533–1539.
- Lammertsma AA, Hume SP. Simplified reference tissue model for PET receptor studies. *Neuroimage*. 1996;4:153–158.
- Stabin MG, Sparks RB, Crowe E. OLINDA/EXM: the second-generation personal computer software for internal dose assessment in nuclear medicine. *J Nucl Med*. 2005;46:1023–1027.
- Guo Q, Owen DR, Rabiner EA, Turkheimer FE, Gunn RN. A graphical method to compare the in vivo binding potential of PET radioligands in the absence of a reference region: application to [¹¹C]PBR28 and [¹⁸F]PBR111 for TSPO imaging. *J Cereb Blood Flow Metab*. 2014;34:1162–1168.
- Delbeke D, Coleman RE, Guiberteau MJ, et al. Procedure guideline for tumor imaging with ¹⁸F-FDG PET/CT 1.0. *J Nucl Med*. 2006;47:885–895.
- Cunningham VJ, Rabiner EA, Slifstein M, Laruelle M, Gunn RN. Measuring drug occupancy in the absence of a reference region: the Lassen plot re-visited. *J Cereb Blood Flow Metab*. 2010;30:46–50.
- Slifstein M, Kegeles LS, Gonzales R, et al. [¹¹C]NNC 112 selectivity for dopamine D1 and serotonin 5-HT(2A) receptors: a PET study in healthy human subjects. *J Cereb Blood Flow Metab*. 2007;27:1733–1741.
- Abi-Dargham A, Martinez D, Mawlawi O, et al. Measurement of striatal and extrastriatal dopamine D1 receptor binding potential with [¹¹C]NNC 112 in humans: validation and reproducibility. *J Cereb Blood Flow Metab*. 2000;20:225–243.
- Kosaka J, Takahashi H, Ito H, et al. Decreased binding of [¹¹C]NNC112 and [¹¹C]SCH23390 in patients with chronic schizophrenia. *Life Sci*. 2010;86:814–818.
- Hirvonen J, Nagren K, Kajander J, Hietala J. Measurement of cortical dopamine D₁ receptor binding with [¹¹C]SCH23390: a test-retest analysis. *J Cereb Blood Flow Metab*. 2001;21:1146–1150.